[Invited] On the impact of launch power optimisation and transceiver noise on the performance of ultra-wideband transmission systems

H. BUGLIA*, E. SILLEKENS , A. VASYLCHENKOVA , P. BAYVEL , AND L. GALDINO

Optical Networks Group, UCL (University College London), Department of Electronic & Electrical Engineering
Torrington Place, London WC1E 7JE, UK
** Corresponding author: henrique.buglia.20@ucl.ac.uk*

Compiled April 28, 2022

Ultra-wideband (UWB) transmission is a promising and cost-effective solution to meet the increasing demand for data traffic in optical fibre systems. However, system performance and quality of transmission (QoT) are limited by fibre nonlinearity, in particular, inter-channel stimulated Raman scattering (ISRS), leading to a power transfer from short to long wavelengths. As the result, per-channel launch power optimisation is required to maximise the system throughput. In this paper, we investigate how the transceiver noise and launch power optimisation impact the total throughput and the per-channel QoT for transmissions bandwidths of up to 20 THz, using S-, C- and L-bands. To measure the gains through the optimum launch power profile, a spectrally uniform launch power is used as a baseline. Through experimental analysis and theoretical modelling, the main limitations constraining the achieved data throughput of 178 Tbit/s over a continuous bandwidth of 16.83 THz and 40 km were investigated. The impact of the launch power optimisation and the transceiver constrained signal-to-noise ratio (SNR) are analysed and compared and the approaches to overcome data throughput limitations are considered. An extensive theoretical investigation for different systems configurations is described, demonstrating the trade-off between ISRS impact and transceiver noise. The former degrades the QoT and increases the gains in performance obtained by optimising the launch power, while the latter reduces these gains and the SNR variation across the bandwidth, with a major impact over short distances.

http://dx.doi.org/10.1364/ao.XX.XXXXXX

1. INTRODUCTION

Over the last decades, the exponential increase of data traffic in optical fibre communication networks has led to the development of new strategies to satisfy this growing demand. Among these strategies, the extension of fibre transmission bandwidth beyond C+L band - also known as ultra-wideband (UWB) wavelength division multiplexing (WDM) - has the greatest potential. It both allows the full exploitation of the existing single-mode fibre (SMF) infrastructure, and extending the use of any future fibre infrastructure. In addition, this approach can co-exist with spatial division multiplexing.

However, UWB operation also requires optical amplifiers covering the entire transmission bandwidth. Erbium-doped fibre amplifiers (EDFA) which enabled the revolution in optical transmission systems in 1990s and 2000s are either being replaced or used in combination with new optical amplifiers technologies operating beyond C+L bands. These include thulium-doped fibre amplifiers (TDFA), semiconductor optical amplifiers (SOA) and distributed Raman amplification [1–12], which have been used over the past few years to achieve milestones of data throughput in SMF over different distances, as shown in Figure 1.

Although bandwidth expansion can lead to higher data throughputs, nonlinear effects, including inter-channel stimulated Raman scattering (ISRS), must be taken into account in the estimation of the distortion due to fibre nonlinear interference (NLI). ISRS effectively results in the power transfer from shorter to longer wavelengths. This power transfer leads to additional complexity in the estimation of the NLI as this depends on the

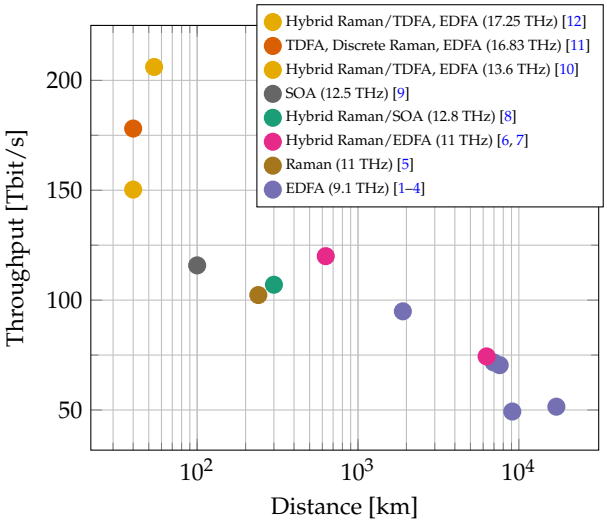

Fig. 1. Record data throughput versus distance for single mode fibre, not including spectral gaps between amplifier gain bandwidths.

evolution of the per-channel launch power. The combination of signal power transfer due to ISRS together with wavelength-dependent attenuation and amplifier noise, the WDM channels, especially from different bands, experience different accumulated distortion. The estimate of the per-channel launch power that maximises the total system performance, also known as launch power optimisation, is thus a multidimensional non-convex problem [13].

The importance of launch power setting in UWB systems was initially discussed in the late 1990's [14–16]. However, recent development of fast and accurate models and algorithms have enabled its computation, including global optimisation algorithms such as evolutionary algorithms (EA) [17, 18], particle swarm optimisation (PSO) [19], artificial neural network (ANN) [20] and faster but sub-optimal strategies [21]. Most importantly, the speed of these algorithms has been improved through analytical [22, 23], numerical [24, 25], or even ANN [26, 27] models that estimate the NLI in the presence of ISRS. These works have all assumed an ideal transceiver subsystem (TRX), and do not allow for the assessment of the impact of TRX noise on the per-channel QoT in the presence of ISRS. This analysis is important to help identify potential performance bottlenecks and over-engineered power control strategies.

In this paper [1], we present a comprehensive analysis of the main noise sources and power optimisation constraints of the UWB transmission experiment published in [11]. We investigate the main limitations that dictated the experiment data throughput of 178 Tbit/s. In particular, we focus on how the TRX noise together with the launch power profile impacted the per-channel QoT and overall data throughput.

This analysis is then broadened to account for different values of TRX noise and other optical fibre transmission system configurations, including the overall transmission distance, the span length and the bandwidth. We have analysed how different amounts of per-channel transferred power due to ISRS change the QoT and the gains in performance obtained by launch power optimisation in the presence of TRX noise. These gains are quantified against the case of a spectrally uniform launch power that does not account for the ISRS effect.

The ISRS Gaussian noise (ISRS GN) model was used to estimate the NLI impact and the resulting per-channel SNR for assessing the system performance. The ISRS GN model is well suited for computing the NLI in UWB transmission systems, and its accuracy compared to the nonlinear Schrodinger equation (NLSE) simulations has previously been demonstrated in [22, 28].

The remainder of the paper is organised as follows. Section 2 describes the analytical model used to estimate the transmission system performance and the launch power optimisation strategy adopted to estimate the per-channel launch power. Section 3 analyses the performance constraints of experiment described in [11], highlighting the potential improvements in system performance. Section 4, extends the analysis for different system configurations with different values of TRX noise and distances. Finally, in Section 5, the impact of span lengths and transmission bandwidth on the QoT, obtained by the launch power optimisation, is studied and quantified. Section 6 summarises the key results and describes the proposed plans and challenges for future work.

2. PRELIMINARIES

This section describes the analytical model and the launch power optimisation strategy adopted throughout this paper to estimate the system performance and the per-channel launch power.

A. Analytical Model

This section describes the analytical model to estimate the transmission system performance. To that end, the impairments arising from the TRX, optical amplifiers to compensate for the fibre loss, and fibre nonlinearity need to be taken into account. Assuming that all these three impairment factors can be modelled as statistically independent additive noise sources, the total received SNR for the ith WDM channel (SNR_i) after N spans is expressed as

$$\mathrm{SNR}_i^{-1} \approx \mathrm{SNR}_{\mathrm{TRX}}^{-1} + \mathrm{SNR}_{\mathrm{ASE}}^{-1} + \mathrm{SNR}_{\mathrm{NLI}}^{-1} = \left(\frac{P_i}{\kappa_i P_i + N P_{\mathrm{ASE}_i} + \eta_N(f_i) P_i^3} \right)^{-1}, \quad (1)$$

where $\mathrm{SNR}_{\mathrm{TRX}}$, $\mathrm{SNR}_{\mathrm{ASE}}$ and $\mathrm{SNR}_{\mathrm{NLI}}$ is the SNR from the transceiver subsystem or back-to-back implementation penalty, the amplified spontaneous emission (ASE) from the optical amplifier used to compensate for the fibre loss and the accumulated NLI, respectively. N is the number of spans, i is the channel under consideration, P_i is its launch power, $\kappa_i = 1/\mathrm{SNR}_{\mathrm{TRX}_i}$, P_{ASE_i} is the ASE noise power, and $P_{\mathrm{NLI}_i} = \eta_N(f_i) P_i^3$ is the NLI noise power after N spans. Note that, in deriving Eq. (1) and for all the calculations and simulations within this paper, we assume that the link under study is made up of identical spans in terms of fibre parameters (the homogeneous link assumption), and that each amplifier compensates for the fibre loss (transparent link assumption) and perfectly equalize the spectral tilt induced, due to the ISRS, in each span, such that the launch power at the beginning of each span is the same for the whole link. We also assume the fibre dispersion is compensated at the end of the link.

The P_{ASE_i} from each amplifier at the frequency of the ith channel is calculated as

[1]This manuscript is an extension of the work presented at the 2021 Optical Network Design and Modelling (ONDM) conference [19]).

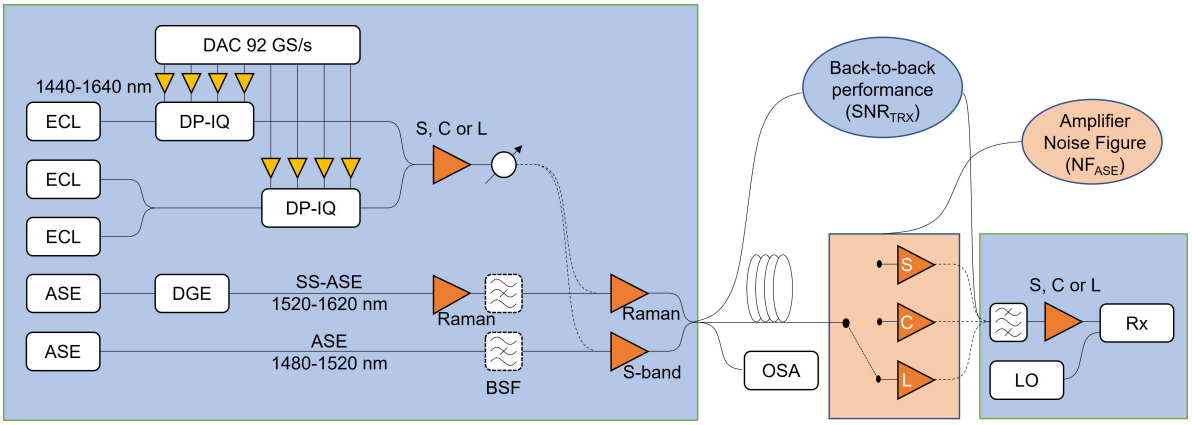

Fig. 2. Schematic of the transmission experiment of [11]. Key: Dynamic Gain Equaliser (DGE), Spectrally Shaped Amplified Spontaneous Emission Noise (SS-ASE), Bandstop Filter (BSF), External Cavity Laser (ECL), Amplified Spontaneous Emission (ASE) noise, Dual-Polarization In-phase Quadrature (DP-IQ) optical modulator, Optical Spectrum Analyser (OSA), Local Oscillator (LO), Digital-to-Analogue Converter (DAC), Receiver (Rx).

$$P_{\mathrm{ASE},i} = 2(G_i - 1)n_{sp}h(f_c + f_i)B_i, \tag{2}$$

where $n_{sp} \approx \frac{NF}{2}$ is the spontaneous emission factor, h is Planck constant, f_c is the reference frequency, and $G_i = P_i(L)/P_i(0)$ is the amplifier gain at the frequency of the ith channel, where $P_i(0)$ and $P_i(L)$ are the powers of channel i at the input and output of the span, respectively.

The NLI coefficient $\eta_N(f_i)$ experienced by the channel of frequency f_i is calculated using the ISRS GN model [24]. This (generalised) model is derived by accounting for the ISRS impact in the GN model [29]. In order to speed up computations, closed-form expressions obtained from the ISRS GN model are used [22]. These closed-form expressions are also generalised to account for arbitrary modulations formats. This is done based on the so-called excess kurtosis (Φ_k), which is set according to the modulation used [30]. The accuracy of these expressions compared to NLSE simulations has been demonstrated at [22, 30]. Based on these closed-form expressions and assuming that the launch power per channel is the same for every span, $\eta_N(f_i)$ can be calculated as

$$\eta_N(f_i) \approx \eta_{\mathrm{SPM}}(f_i) + \sum_{k=1,k\neq i}^{N_{\mathrm{ch}}} \eta_{\mathrm{XPM,k}}(f_i), \tag{3}$$

where N_{ch} is the number of channels, $\eta_{\mathrm{SPM}}(f_i)$ is the contribution to the NLI from self-phase modulation (SPM) and $\eta_{\mathrm{XPM,k}}(f_i)$ is the contribution from cross-phase modulation (XPM) from each kth WDM channel. The closed-form expressions for η_{SPM} and η_{XPM} are, respectively [30]:

$$\eta_{\mathrm{SPM}}(f_i) = \frac{4}{9}\frac{\pi\gamma^2 N^{1+\epsilon}}{B_i^2\phi_i\tilde{\alpha}_i(2\alpha_i+\tilde{\alpha}_i)}\left[\frac{T_i-\alpha_i}{\alpha_i}\mathrm{asinh}\left(\frac{\phi_i B_i^2}{\pi\alpha_i}\right) + \right.$$
$$\left. + \frac{A_i^2 - T_i}{A_i}\mathrm{asinh}\left(\frac{\phi_i B_i^2}{\pi A_i}\right)\right], \tag{4}$$

where γ is the nonlinear coefficient, B_i is the channel bandwidth, ϵ is the coherence factor [Eq. 22, 29] which accounts for the coherent accumulation of the nonlinearity, α_i and $\tilde{\alpha}_i$ are attenuation coefficients, where the latter appears because of the fitting strategy described in [22]. $\phi_i = \frac{3}{2}\pi^2(\beta_2 + 2\pi\beta_3 f_i)$, β_2 and β_3 are respectively the group velocity dispersion (GVD) parameter and its linear slope, where both are assumed to be the same for all the channels. $A = \alpha + \tilde{\alpha}$, $T_i = (\alpha + \tilde{\alpha} - P_{\mathrm{tot}}C_{\mathrm{r,i}}f_i)^2$, P_{tot} stands for the total power injected into the fibre and $C_{r,i}$ is the slope of the linear regression of the normalised Raman gain spectrum, obtained by assuming a triangular-shape profile [31], and

$$\eta_{\mathrm{XPM,k}}(f_i) = \frac{32}{27}\left(\frac{P_k}{P_i}\right)^2\frac{\gamma^2}{B_k}$$
$$\left\{\frac{N+\frac{5}{6}\Phi_k}{\phi_{ik}\tilde{\alpha}_k(2\alpha_k+\tilde{\alpha}_k)}\left[\frac{T_k-\alpha_k^2}{\alpha_k}\mathrm{atan}\left(\frac{\phi_{ik}B_i}{\alpha_k}\right) + \right.\right.$$
$$\left. + \frac{A_k^2 - T_k}{A_k}\mathrm{atan}\left(\frac{\phi_{ik}B_k}{A_k}\right)\right] + \frac{5}{3}\frac{\Phi_k\pi\tilde{N}T_k}{|\phi|B_k^2\alpha_k^2A_k^2}$$
$$\left.\left[(2\Delta f_{ik} - B_k)\log\left(\frac{2\Delta f_{ik}-B_k}{2\Delta f_{ik}+B_k}\right)2B_k\right]\right\}, \tag{5}$$

with $\Delta f_{ik} = |f_k - f_i|$, $\phi_{i,k} = 2\pi^2(f_k - f_i)[\beta_2 + \pi\beta_3(f_i + f_k)]$, $\phi = -4\pi^2[\beta_2 + \pi\beta_3(f_i + f_k)]L$ and $\tilde{N} = 0$ for single span or $\tilde{N} = N$ otherwise. Note that although Eqs. (4) and (5) are obtained using the triangular Raman spectrum approximation and the assumptions described in [22], these equations can be used with the true Raman spectrum and in more general scenarios. These scenarios include, regions beyond the triangular approximation of the Raman gain spectrum, i.e, beyond 15 THz, or even if some of these assumptions are not satisfied (eg. the case of spectrally non-uniform launch power distributions and wavelength-dependent attenuation). This is done by matching the parameters α, $\tilde{\alpha}$ and C_r to the actual power profile of each interfering channel, obtained by solving the differential Raman equations [Eq. 2, 28].

Additionally, as the power of each channel is related to the power of the remaining channels, this optimisation needs to be carried out jointly, resulting in a multidimensional optimisation problem. It is also shown in [13] that, because of ISRS, this optimisation is non-convex. Given this nonlinear dependency, it is appropriate to use global optimisation algorithms. Throughout this paper, we used the particle swarm optimisation (PSO) [32] combined with a gradient descent algorithm with a back straight line search [Chap. 9, 33]. This provides a good balance between local and global search and is explained in more detail in Section 2.B.

Finally, for any optical transmission system, the total throughput is bounded above by the additive white Gaussian noise (AWGN) channel capacity [34] given by:

$$C_{\text{Total}} = \sum_{i=1}^{N_{\text{ch}}} C_i = \sum_{i=1}^{N_{\text{ch}}} 2 \cdot \log_2(1 + \text{SNR}_i), \quad (6)$$

where SNR_i is obtained from Eq. (1) and C_i is the AWGN capacity for the ith channel.

B. Launch Power Optimisation

This section describes the algorithm used for launch power optimisation. Due to the ISRS, the relation between system performance and launch power is nonlinear, leading to a N_{ch}-dimensional non-convex optimisation problem [13]. To solve this problem, numerical optimisation algorithms are required.

Our goal is to find the optimum launch power allocation P_i for the transmitted channels, maximising the total throughput for the transmission system. The total throughput is bounded above by the AWGN channel capacity, thus we choose Eq. (6) as our cost function to be maximised for a set of values of P_i, with SNR_i for the ith channel given by Eq. (1). Note that, this optimisation is independent of the TRX, i.e, the launch power profile which maximises Eq. (6) is the same for any value of SNR_{TRX}.

The numerical optimisation algorithms chosen to find a local maximum of Eq. (6) in this paper are the PSO [32] combined with a gradient descent algorithm with a backtracking line search to determine the step size. The PSO is efficient in exploring the N_{ch}-dimensional space, leading to the surroundings of a good local optimal solution on the N_{ch}-dimensional surface. In order to accurately find this solution, the gradient descent algorithm is used with the initial condition as the solution of the PSO.

For the PSO, we use the Matlab function provided by the global optimisation toolbox. We choose $10 \cdot N_{\text{ch}}$ particles with their values, i.e, the launch power for each channel, ranging from -15 dBm to 15 dBm. The PSO algorithm begins by assigning to these particles uniform distributed random values in this interval, which represent their locations in the N_{ch}-dimensional space. Initial particle velocities are also randomly picked from the interval $[-30, 30]$ dBm and the initial inertia is set to 1.1. The algorithm evaluates the cost function (Eq. (6)) at each particle location, storing the current best solution, which is iteratively used to update particles' velocities and locations. Iterations proceed until the algorithm reaches a stopping criterion, which we choose to be a maximum of 100 interactions. For the gradient descendent algorithm, a convergence rate of 10^{-3} is chosen and for the backtracking line search we set $\alpha = 0.15$ and $\beta = 0.8$ [Chap. 9, 33]. Additionally, adjacent channels are lumped together into one super-channel in order to reduce computational complexity - this approach is justified by the fact that adjacent channels are likely to have similar launch power.

In addition to the optimum launch power per channel, we also use this strategy to calculate the optimum spectrally uniform launch profile, such that each channel carries the same launch power. This is computed considering 1 super-channel for the entire bandwidth with the attenuation coefficient as equal to the central channel. This approach leads to a single-dimensional space and omits the impact of the ISRS as just 1 super-channel is transmitted.

Table 1. Amplification scheme sub-bands with corresponding noise properties and implemented modulation formats, used in the experiment [11] and its modelling.

Sub-band [nm]	NF_{ASE} [dB]	GS-QAM	SNR_{TRX} [dB]
1484.86 - 1519.8	7.0	256-QAM	15.80
1520 - 1529	9.0	64-QAM	17.82
1529.2 - 1568	5.5	1024-QAM	21.25
1568.2 - 1607.8	6.0	1024-QAM	21.25
1608 - 1619.67	9.0	256-QAM	17.07

3. PERFORMANCE ANALYSIS OF UWB TRANSMISSION EXPERIMENT

In this section, the model described in Section 2.A is applied to simulate the UWB the experiment described in [11]. This analysis allows us to draw general conclusions about the experiment and to search for ways of potential improvements for future work. This section starts by describing the experimental configuration within the simulation parameters considered to model the experiment, followed by the computation of different launch power profiles, which are compared with the one used in the experiment. For these different launch power profiles, we analyse the system performance in terms of SNR and total throughput. Finally, we investigate the interplay between TRX and launch power optimisation by analysing how the different cases of launch power profiles together with the TRX noise influence the system performance.

A. Configuration

This section describes the parameters of the transmission system used to model the experiment in [11]. The experimental setup is shown in Figure 2. A complete description of the experimental setup can be found in [Sec. 2, 11]. As shown in this figure, the transmitter and receiver impairments are gathered into SNR_{TRX}, which corresponds to the experimental back-to-back implementation penalty [2] as indicated in this figure as the blue background. Similarly, the impairments of the optical amplifiers used to amplify the signal after fibre propagation are described as NF_{ASE}, which is represented by the orange background. Also, in order to calculate the system performance, we use the model and the assumptions presented in Eq. (1).

The experimental transmission system parameters used in the analytical model are summarised in Table 1. The system is based on [11] and it consists of a WDM transmission with N_{ch}=660 channels spaced by 25.5 GHz. Each channel was modulated at the symbol rate of 25 GBd. This results in a total bandwidth of 16.83 THz (134.81 nm), ranging from 1484.86 nm to 1619.67 nm, corresponding to the continuous transmission over S-, C- and L-bands. The channels are transmitted over a single span of 40 km standard SMF with attenuation profile $\alpha(f_i)$ as [Fig. 2, 11]. Total power of 20.4 dBm is launched into the fibre and the power per channel is shown in Figure 3 by the red line. Note that, no dynamic gain equaliser (DGE) was available to equalise the power for lower wavelengths (from 1484.86 nm to 1520 nm), therefore the signal gain followed the amplifier

[2] The transceiver impairment is modelled as AWGN. The SNR_{TRX} is calculated as $\frac{\mathbb{E}[|X|^2]}{\mathbb{E}[|Y-X|^2]}$, where $\mathbb{E}[\cdot]$ is the expectation operator, X is the transmitted symbols and Y the received symbols after digital signal processing.

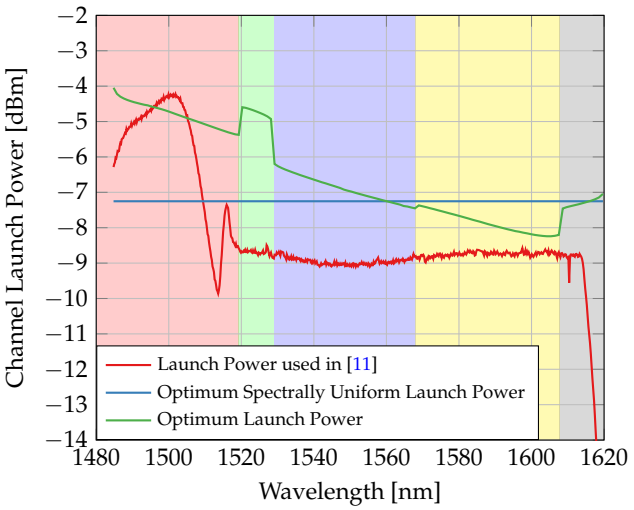

Fig. 3. Launch power per channel obtained from the optimisation strategy described in Section 3.B, using the model proposed in Section 2.A. The launch power used in [11] (red) is also shown for comparison.

ASE power profile. For the remaining wavelengths, a spectrally uniform power profile was used.

For the in-line amplifiers shown in Figure 2 (orange background), the noise figure values (NF_{ASE}) are the ones reported in [Sec. 2, 11] and displayed in Table 1. The back-to-back implementation penalty (SNR_{TRX}) has not been measured experimentally for every channel. For each amplifier sub-band, the SNR_{TRX} of 3 channels were measured and their mean value was used, as shown in Table 1, as an estimate of the per-channel SNR_{TRX}.

The same geometrically-shaped (GS) quadrature amplitude modulation (GS-QAM) formats of [11], which were optimised based on the received SNR, were also taken into account to estimate the SNR_{NLI} in the modelling. This is done by using different values of Φ_k in Eq. (5), according to the GS-QAM constellation used per amplification sub-band, which is also shown in Table 1. The constellation diagrams of these GS-QAM constellations are shown in [Fig. 3, 11]. Furthermore, these constellations are also used to estimate the total throughput of the system based on the generalised mutual information (GMI).

B. Launch Power Profiles

The next step is to quantify the optimum and the spectrally uniform launch power profiles using the strategy described in Sec 2.B. For this, five adjacent channels were lumped together into joint super-channels to reduce computational complexity.

Figure 3 shows the optimum launch power (green line), with a total power of 21.93 dBm, as well as the signal power profile used on the experiment [11] (red line), with a total launch power of 20.4 dBm. For the spectrally uniform power (blue line), a total launch power of 20.95 dBm, corresponding to a -7.25 dBm per channel, was found. For ease of viewing, different background colours are used to mark the different values of NF_{ASE} for the in-line amplifiers used across different sub-band within the gain bandwidth as shown in Table 1.

For the optimum launch power profile (green line), the maximum power value of -4 dBm is found at 1484.86 nm and minimum power value of -8.2 dBm at 1607.8 nm, resulting in a maximum per-channel launch power variation (ΔP) of 4.2 dB across the bandwidth. Such variation can be understood by noting that due to ISRS, $\eta_N(f_i)$ is higher for longer wavelengths, even though these wavelengths experience greater dispersion. In contrast, P_{ASE_i} is higher for shorter wavelengths, as these wavelengths experience more loss due to the attenuation profile combined with the ISRS. Thus, higher launch power is expected for shorter wavelengths, as these wavelengths experience more ASE noise and less nonlinear effects. Note that, the shape of the wavelength-dependent attenuation profile used [Fig.2, 11], must also be considered in this analysis, which in combination with the power transferred due to the ISRS effect, also changes the distribution of the ASE and NLI noise powers among the channels.

Foremost, as described in detail in [11], different amplification technologies, such as Thulium-doped fibre, discrete Raman and Erbium-doped fibre amplifiers, are utilised for different wavelengths ranges within the total transmission bandwidth. Each amplifier determines its operational wavelength ranges and demonstrates different NF_{ASE} values, as shown in Table 1. Therefore, we observe humps in the optimal power profile at different sub-bands highlighted by the different background colours, while maintaining the main trend of a downward slope. Indeed, to neutralise the undesired impact of higher ASE noise from the in-line amplifiers, higher launch power is required.

C. Transmission System Performance

In this section, we analyse the experimental and theoretical performance of the transmission configuration described in Section 3. The SNR is used as performance metric and the three launch power profiles shown in Section 3.B are used to estimate the system performance based on Eq. (1). Additionally, in order to analyse how the TRX noise impacts the transmission system performance for each studied launch power profile, we also included the case of an ideal TRX by setting $SNR_{TRX} = \infty$ for the entire transmission bandwidth in our analysis. Both cases are shown in Figure 4.

Figure 4 (a) shows the received SNR (Eq. (1)) with the inclusion of the noise introduced by the experiment back-to-back implementation penalty, as per Table 1 for the different launch power profiles. Note that, all the three launch power profiles considered, yield pretty much the same per-channel SNR, as all the three continuous lines almost overlap completely. This proves that the transmission system performance under investigation is mainly limited by the transceiver noise. This is because Eq. (1) is dominated by the SNR_{TRX} term. As the TRX impact is purely characterised by the back-to-back SNR, the launch power optimisation does not have a considerable impact on the system performance after 40 km fibre transmission.

The experimentally measured received SNR from [11] is shown as grey markers for comparison, average error of 0.52dB is found between the continuous lines and the grey markers, showing a good agreement between the analytical model, described in Section 2.A, and the experimental results.

In contrast, Figure 4 (b) shows the SNR obtained by considering an ideal transceiver ($SNR_{TRX} = \infty$). For the optimum launch power profile (green line), the SNR varies between 31.59 dB and 35.37 dB. For the spectrally uniform launch power profile (blue line), the SNR varies between 30.28 dB and 35.32 dB. For both cases, the minimum and maximum value of SNR occurred at 1607.8 nm and 1529.2 nm, respectively. This difference is because for an ideal transceiver, Eq. (1) is dominated by SNR_{NLI} and SNR_{ASE} which are both dependent on the launch power

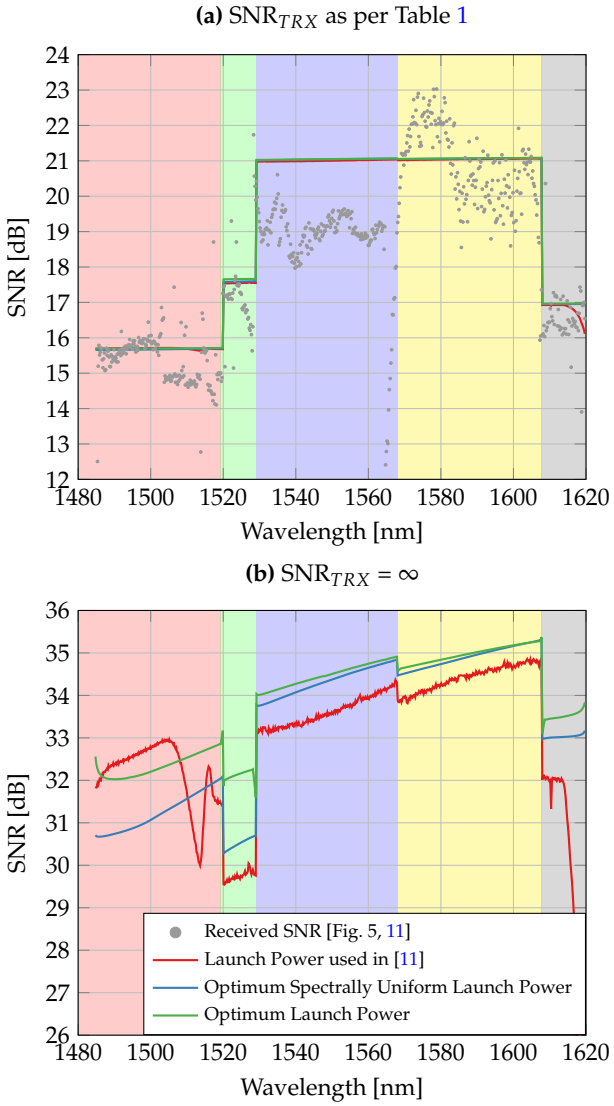

Fig. 4. Per-channel SNR profile for the different launch power profiles shown in Figure 3. Two scenarios are considered: (a) transceiver noise as Table 1 and (b) the case of an ideal transceiver. The experimental measurements in [11] (grey marks) are shown for comparison.

profile. Similar to Section 3.B, the humps (green curve) observed in the SNR profile at different sub-bands highlighted by the different background colours, rely on the different in-line amplifier NF_{ASE} used to compensate for fibre loss. Furthermore, the main trend of an upward slope is observed as the lower wavelength channels experience the lowest SNR values due to ISRS.

For the launch power used in the experiment (red line), the SNR varies between 23.18 dB at 1619.67 nm and 34.86 dB at 1607.8 nm. This represents a maximum per channel SNR variation of 11.68 dB across the entire transmission bandwidth, compared to only 3.78 dB for the optimum launch power profile case. Note that, for channels in the range of 1487-1508 nm, the SNR values are higher for the experiment case. This is due to the combination of two factors when compared with the optimum launch power per channel profile. Firstly, because of their increased per-channel launch power values in this wavelength range. Secondly, because these channels transfer less power to

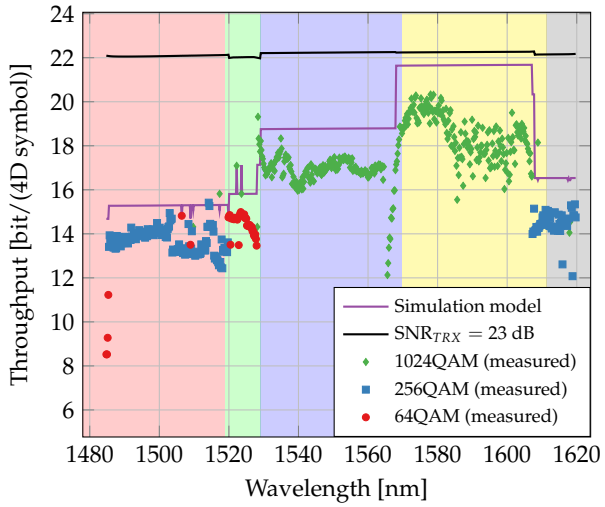

Fig. 5. Per-channel data throughput after 40 km transmission, estimated using the Monte-Carlo integration as [Eq. 36, 35] with the GS-QAM constellations designed in [Fig.3, 11] (purple line). The experimental measurements in [11] (marks) and the scenario of a better TRX performance $SNR_{\mathrm{TRX}} = 23$ dB (black line) are shown for comparison.

the longer wavelengths channels. The latter occurs because of the reduced launch power used for channels above 1520 nm. This decreases the performance of these channels in exchange of an increase in performance for the channels between 1487 nm - 1508 nm. As a result, a lower mean SNR is obtained for the launch power used in the experiment compared with the other launch power profiles.

D. Data Throughput

In this section, we analyse the system performance in terms of throughput. The values of SNR estimated for each studied launch power profile are used to calculate the achievable information rate (AIR) and the GMI is used as a metric for AIR. The GMI is calculated using the Monte-Carlo integration as [Eq. 36, 35], and the GS-QAM constellations designed in [Fig.3, 11] were used depending on the received SNR (see Table 1). Additionally, as in the experiment, a pilot overhead of 4.64% is accounted for in the calculations.

Figure 5 shows the experimental measurements and theoretical calculations of the per-channel throughput, obtained by multiplying the estimated GMI by the pilot overhead. Total throughput of 194.55 Tbit/s is obtained, against 178.08 Tbit/s reported in [11]. This discrepancy is explainable by some modelling assumptions, e.g., flat noise figures across each amplifier bandwidth gains, the SNR_{TRX} was measured for a few channels only, and constant NF assumption was made for the other channels.

It is important to stress that this large variation in the back-to-back performance across different bands (see Table 1) is mainly

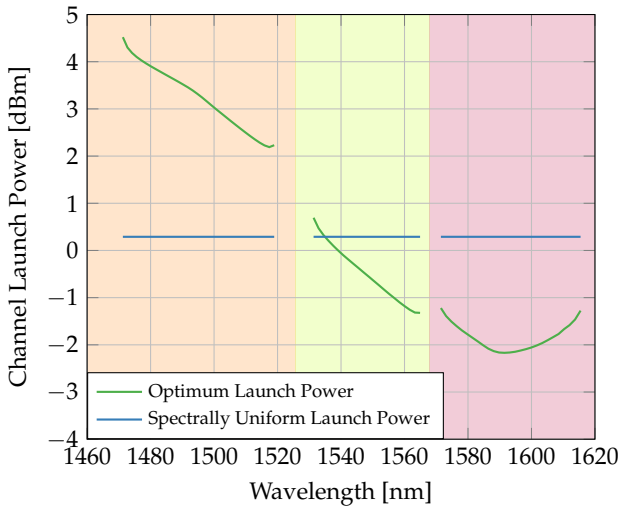

Fig. 6. Optimum (green curve) and spectrally uniform (blue curve) launch power per channel optimised for a single span.

due to experimental setup constraints [3], especially for the S-band wavelengths. In a deployed system, with individual transponders per channel, a similar level of $\mathrm{SNR}_{\mathrm{TRX}}$ across all WDM channels would be expected. Therefore, in order to investigate what could potentially be the throughput if there were no experimental constraints, we computed the throughput for a realistic value $\mathrm{SNR}_{\mathrm{TRX}} = 23$ dB for all channels (continuous black line in Figure 5).

For this case, we optimised the launch power for the GS-1024 QAM constellation shown in [Fig. 4, 11], which based on the received SNR it was found to be the optimum choice from three possible constellations for all the bands. A total throughput of 232.47 Tbit/s is obtained, indicating that a considerable improvement in the total throughput with respect to [11] could potentially be achieved.

4. INTERPLAY BETWEEN TRANSCEIVER NOISE AND LAUNCH POWER OPTIMISATION IMPACTS ON OVERALL SYSTEM PERFORMANCE

This section explores the impact of launch power optimisation on the per-channel system performance and quality of transmission (QoT) for different values of $\mathrm{SNR}_{\mathrm{TRX}}$ and distances spanning from short to metro, long-haul and trans-Atlantic. For this, a more practical system configuration, that takes into account commercial optical amplifiers gain bandwidth and high symbol rate transponders was considered.

The transmission system is assumed to have $N_{\mathrm{ch}} = 183$ WDM channels centered at 1540 nm, ranging from 1471.3 nm to 1615.5 nm. Each channel was modulated at the symbol rate of 96 GBd and is spaced by 100 GHz from its neighbour. We consider the utilisation of S-, C- and L-bands together with spectral

[3]Two different types of lasers for the LO were used in this experiment: external cavity laser (ECL) with 15.5 dBm output power and 100 kHz linewidth was used for wavelengths between 1529.2 nm to 1607.8 nm. For the remaining wavelengths, ECL with 300 kHz linewidth and 0 dBm output power followed by an optical amplifier was used to operate the receiver at optimum power. Further, due to a limited number of TDFAs, SOA had to be used to pre-amplify the received signal for S-band wavelengths, incurring an SNR penalty for the S-band channels (1484.86 nm to 1519.8 nm). A significant penalty in the back-to-back performance was also measured for the wavelength bands (from 1520 nm to 1529 nm and from 1608 nm to 1619.67 nm) that used discrete Raman amplifiers to compensate for the transmitter and receiver losses.

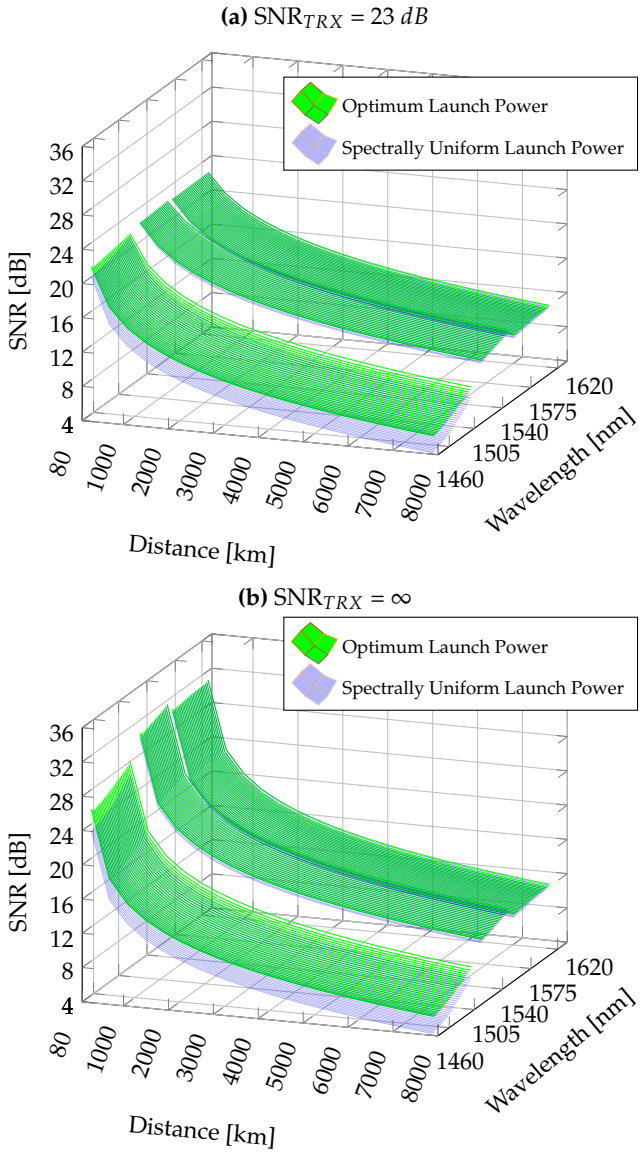

Fig. 7. Per channel SNR profile for different distances and for the different launch power profiles shown in Figure 6. Two scenarios are considered: (a) non ideal transceiver with $\mathrm{SNR}_{\mathrm{TRX}} = 23$ dB and (b) the case of an ideal transceiver.

gaps between each band. For the S/C and C/L separation bands, we consider gaps of 10 nm and 5 nm, respectively. The noise figures of each band are 7 dB, 4 dB, and 6 dB in the S-, C- and L-band, respectively. For simplicity, we consider Gaussian constellations (i.e., $\Phi_k = 0$), such that each span is made of 80 km SMF (same fibre parameters of Section 3) and the fibre launch power of each WDM channel to each span was controlled to the target value by assuming adaptive spectral equalisation and dynamic gain control of the amplifiers. The latter allows the application of the model described in Section 2.A to remain valid.

Due to the assumption of coherent accumulation of the nonlinearity ($\epsilon \neq 0$), the optimum and the spectrally uniform launch power per channel are not exactly the same for every span. However, $\epsilon \to 0$ as the number of channels increases [Fig. 10, 29]. Using this assumption, we optimised the launch power for a single span and used this same launch power as an approximate

optimum launch power for every span. The optimum launch power per channel and the spectrally uniform launch power profile are shown in Figure 6. Both launch power cases are obtained using the same strategy and the same optimisation parameters of Sections 2.B and 3.B, except that in this case, each 2 adjacent channels are lumped together into 1 super-channel to reduce complexity. For the optimum launch power profile (green curve), a total launch power of 23.68 dBm and a maximum per channel power variation of 6.7 dB (4.5 dBm for 1471.47 nm and -2.17 dBm for 1591.47 nm) are found. For the spectrally uniform launch power (blue curve) a total launch power of 22.91 dBm is obtained, with 0.29 dBm per channel. Note that, for the optimum launch power profile case, there is an increase in the channel powers for wavelengths above 1590 nm. This is because the ISRS effect is drastically reduced for spectral spacing above 15 THz. Both launch power profiles strategies are used in this section to estimate the transmission system performance.

Figure 7 illustrates the per channel SNR for different transmission distances and launch power profiles. Two cases are considered: per channel $SNR_{TRX} = 23$ dB (a) and an ideal transceiver, with $SNR_{TRX} = \infty$ for all the channels (b). The aim here is twofold. Firstly, to investigate how the SNR_{TRX} value impacts the per-channel SNR for different transmission distances, when transmitting the optimum power per channel (green surface) or the spectrally uniform power (blue surface) profiles. Secondly, to investigate how the SNR_{TRX} value impacts the quality of transmission (QoT) across the entire transmission bandwidth. This is measured by analysing the maximum per channel SNR variation across the entire bandwidth (designated as ΔSNR).

When comparing Figure 7(a) with Figure 7(b), it can be noticed that SNR_{TRX} reduces the transmission performance difference between the launch power profile cases. For instance, in case (a), for 80 km, the average SNR are respectively 21.93 dB and 21.62 dB for the optimum power and spectrally uniform power profile, respectively. This corresponds to a difference of only 0.31 dB SNR, while the same analysis for case (b) results in 28.96 dB and 28.08 dB, corresponding to a difference in SNR between both launch power profiles of 0.88 dB. Moreover, it can be seen that SNR_{TRX} yields a flatter QoT for both launch power profiles by reducing the maximum per channel SNR variation (ΔSNR) across the bandwidth. For instance, in the case (a) for 80 km, the ΔSNR is 1.39 dB and 2.33 dB for the optimum and the spectrally uniform launch power profiles, respectively. The same analysis for the case (b) ($SNR_{TRX} = \infty$) results in a ΔSNR of 6.14 dB and 8.23 dB, respectively.

In order to further investigate the difference in transmission system performance for both launch power profile cases, Figure 8 shows the SNR gains (a) and throughput gains (b), relative to the spectrally uniform power profile, for the optimum launch power profile. Different values of SNR_{TRX} and transmission distances are considered. The SNR gains are averaged over all the channels and the throughput is computed using the AWGN capacity (Eq. (6)).

It can be noted that in Figure 8, for short distances, the gains in SNR and throughput drop depending on the SNR_{TRX} and this drop is monotonically reduced for long distance. It can also be observed that, for the case of an ideal transceiver ($SNR_{TRX} = \infty$), the slightly reduction in the SNR gain with distance is result of the deviation between the launch power used, which was optimised for a single span only. However as previously explained, due to the coherent accumulation, the optimum launch power slightly drops with the number of spans. Also, note that in Figure 8 (b), the throughput gains increase with distance. This is a result of the logarithmic dependence between SNR and AWGN capacity.

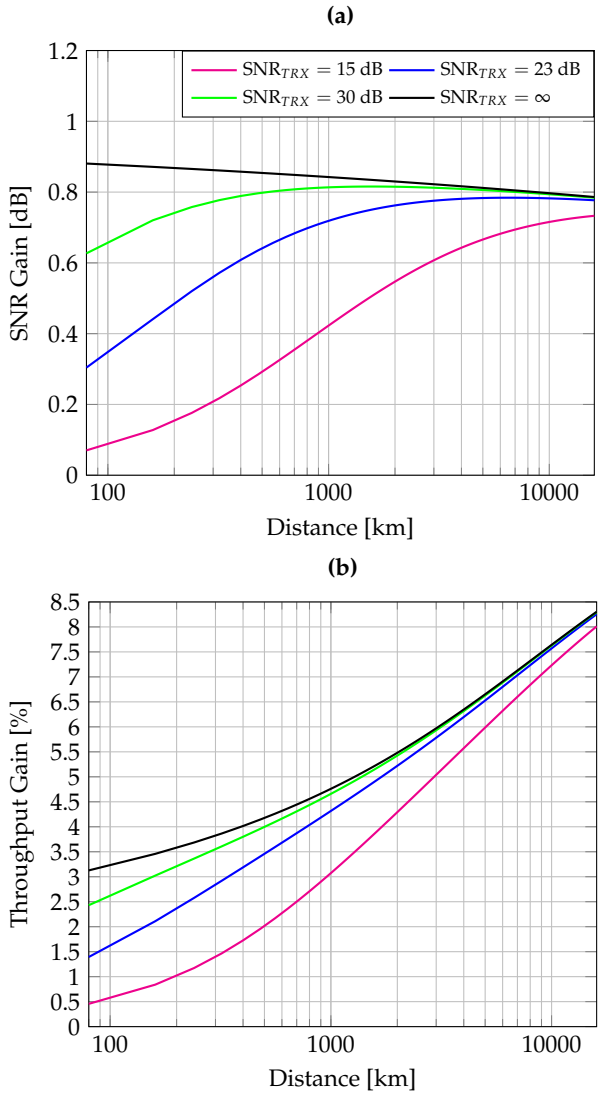

Fig. 8. Gain in SNR (a) and in throughput (b) obtained by using the optimum instead of the spectrally uniform launch power profile. The launch power profiles are shown in Figure 6. The gains are averaged over the channels.

To investigate how the different launch power profiles and the SNR_{TRX} impact the system QoT for different distances, we computed ΔSNR for different values of SNR_{TRX} and distance, and the results are shown in Figure 9. The continuous line illustrates the results for the optimum launch power per channel, while the dashed line shows the results for the spectrally uniform launch power profile. Firstly, it can be noted that the optimum launch power profile improves the QoT by reducing the SNR variation across bandwidth for any distance and SNR_{TRX} value. For the case of an ideal transceiver, this difference is approximately 2 dB for any distance. For a transceiver constrained SNR system, this improvement is reduced for short distances, and increases with distance. Moreover, the lower is the SNR_{TRX}, the more even is the QoT across the channels. This flatness in the QoT is noted with greater impact for short distances and is monotonically reduced as the distance increases.

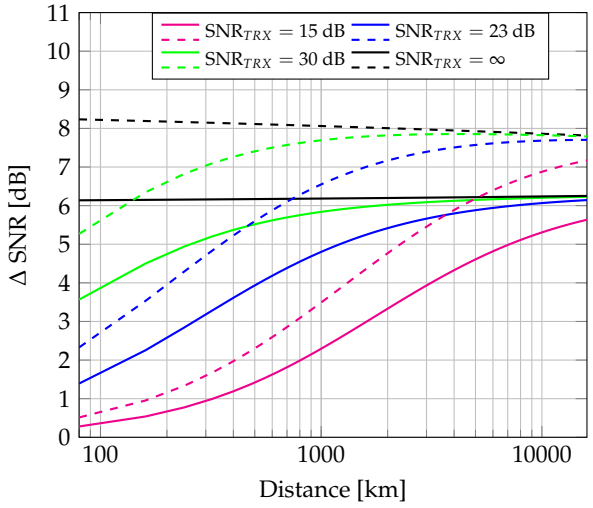

Fig. 9. Maximum per channel SNR variation (ΔSNR), i.e, difference in SNR between the most and the least distorted channel for different values of SNR_{TRX}. Both launch power profile cases shown in Figure 6 are considered, optimum launch power profile (dashed lines) and spectrally uniform launch power profile (continuous lines).

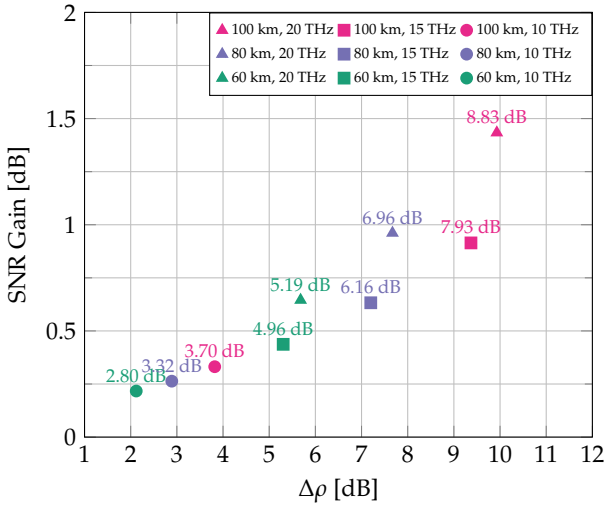

Fig. 10. The gain in SNR as function of the maximum transferred power between channels (Δρ) due to ISRS, for each of the scenarios shown in the legend. For each scenario, the maximum launch power per channel variation (ΔP) is shown above the marker. The gains in SNR are averaged over the channels and computed for a single span.

In summary, when the TRX noise is the main source of impairment in the system, the gains provided by the utilisation of the optimal, instead of the spectrally uniform launch power, is reduced as SNR_{TRX} is the same, irrespective of the launch power per channel.

5. IMPACT OF LAUNCH POWER OPTIMISATION ON DIFFERENT SPAN LENGTHS AND TRANSMISSION BANDWIDTHS

In this section, we investigate how the QoT and the gains in performance, obtained by using the optimum instead of the spectrally uniform launch power profile, change for different span lengths and transmission bandwidths. All analyses are carried out in the absence of the TRX noise contribution, ($SNR_{TRX} = \infty$) and for a single span. This is because the impact of TRX in the SNR gain and ΔSNR has been demonstrated in Section 4 and can be easily extended for the scenarios considered in this section.

The system configurations considered here is the same as in Section 4, but with span lengths of 60 km, 80 km and 100 km, and bandwidths of 10 THz, 15 THz and 20 THz, corresponding to transmissions of 101, 151 and 201 channels centered at 1540 nm, respectively. For each of these system scenarios, the optimum and the spectrally uniform launch power profiles are computed following the strategy of Section 2.B, and these launch power profiles are used to estimate the SNR gain and the SNR variation across the bandwidth ΔSNR. In order to analyse how the different span lengths and bandwidths change the level of the ISRS effect, we also compute, for each case, the maximum ISRS-transferred power Δρ. This is done by computing the difference between the maximum and the minimum values of the Raman transfer function.

For the different transmission bandwidths and span lengths considered in this section, Figure 10 shows the gains in terms of SNR between the optimum and the spectrally uniform launch power profiles as a function of the maximum transferred power between channels (Δρ) due to ISRS. Also, for each case, we

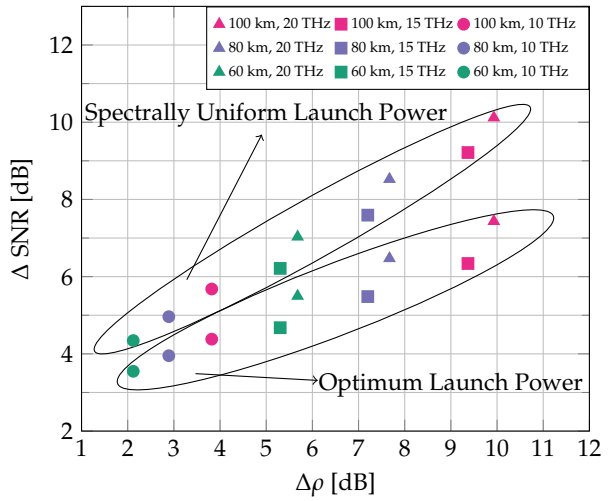

Fig. 11. Maximum per channel SNR variation (ΔSNR), i.e, the difference in SNR between the most and the least distorted channel as s function of the maximum transferred power between channels (Δρ) due to ISRS, for the different scenarios shown in the legend. For each scenario, ΔSNR is shown for the optimum (lower ellipse) and the spectrally uniform (upper ellipse) launch power profiles.

indicate the value of per-channel launch power variation (ΔP) above each marker. It can be noted an upward trend between the strength of ISRS impact measured by the maximum transferred power between channels (Δρ) and the SNR gains achieved by the power optimisation. This is because a larger amount of power being transferred between channels due to the ISRS effect needs to be compensated for, increasing ΔP. Therefore, the greater is ΔP, the greater is the difference between the per channel launch powers of the optimum and the spectrally uniform profiles, increasing the SNR gains.

Two further observations are remarkable in 10.Firstly, note that for the cases of 60 km and 80 km both with 10 THz, the maximum transferred power between channels due to ISRS is lower than the maximum launch power per channel variation, i.e, $\Delta\rho < \Delta P$, while for the remaining scenarios this trend is reversed, i.e, $\Delta\rho > \Delta P$. This is because the strong ISRS effect flips the NLI profile [Fig. 5, 28], i.e, for increasing ISRS, the magnitude of NLI turns to be higher for the long wavelengths channels, even with these channels experiencing higher levels of dispersion.

Secondly, it should be noted that for some scenarios, the SNR gain is lower even with higher $\Delta\rho$. For instance, for a span length of 80 km and bandwidth of 20 THz, a $\Delta\rho$ of 7.67 dB provides a SNR gain of 0.96 dB, while for a span length of 100 km and bandwidth of 15 THz, a $\Delta\rho$ of 9.37 dB provides a SNR gain of 0.91 dB. To explain it, we can refer to Figure 6. We can notice that, in the spectrally uniform case, the long-wavelength channels experience a higher impact of NLI, because their per-channel power values are larger than the optimal ones. Therefore, it diminishes the SNR gains, despite demonstrating higher values of $\Delta\rho$.

Figure 11 shows the maximum per channel SNR variation (ΔSNR) as a function of the maximum transferred power between channels ($\Delta\rho$) for the different span length and bandwidths. Similar to Section 4, this variation is computed using the optimum (lower ellipse) and the spectrally uniform (upper ellipse) launch power profiles. As expected the ΔSNR variation is reduced when using the optimum power profile instead of the spectrally uniform launch power profile, improving the QoT. More interesting here, is that, firstly, this reduction in ΔSNR follows an upward trend as the strength of ISRS increases. Secondly, ΔSNR increases with $\Delta\rho$, deteriorating the QoT for both the optimum and the spectrally uniform launch power profiles.

6. CONCLUSIONS

Using the analytical modelling together with experimental measurements, we have characterised the impact of the ISRS on the per-channel QoT. In particular, we investigated the interplay between the transceiver constrained-SNR and power control strategies. It was observed that for short and metropolitan distances, the gains achieved by the optimum power optimisation (that takes into account the ISRS effect) compared with spectrally uniform launch power are drastically reduced in the presence of transceiver noise.

The transceiver noise mitigates the impact of the ISRS on the overall data throughput as well as on the per-channel QoT for short and metro networks. Therefore, when designing and modelling a UWB network it is paramount to take into account the transceiver constrained-SNR. This will enable improved understanding of the potential gains achievable by launch power optimisation strategies, and more informed decisions to be made on the trade-off between network design complexity and network performance.

In the optical network context, performance optimisation is an interesting and challenging research topic, as individual links can be populated with a variable number of channels and characteristics. Because of this, future ultra-wideband WDM transmission systems will require the development of open and effective network planning tools. The latter will allow an online assessment of the data rates, modulation formats, the number of channels and launch power profile, given the fibre, the amplifier characteristics and allocated lightpaths. Thus, a natural extension of this work is to broaden the analysis to account for these networking aspects, including different span lengths, the adding/dropping of channels with different accumulated NLI and ASE noise per wavelength channel, as well as dynamic traffic scenarios.

DATA AVAILABILITY STATEMENT

The data that supports the figures in this paper are available from the UCL Research Data Repository (DOI: 10.5522/04/17086559), hosted by FigShare.

FUNDING

This work is partly funded by the EPSRC Programme Grant TRANSNET (EP/R035342/1). H. Buglia is funded jointly by an EPSRC studentship EP/T517793/1 and the Microsoft 'Optics for the Cloud' Alliance. A. Vasylchenkova acknowledges the support of the Leverhulme Trust Early Career Fellowship (ECF-2020-150). L. Galdino is supported by the Royal Academy of Engineering Research Fellowship and a Royal Society Research Grant.

REFERENCES

1. J. . Cai, H. G. Batshon, M. V. Mazurczyk, C. R. Davidson, O. V. Sinkin, D. Wang, M. Paskov, W. W. Patterson, M. A. Bolshtyansky, and D. G. Foursa, "94.9 Tb/s single mode capacity demonstration over 1,900 km with C+L EDFAs and coded modulation," in *European Conference on Optical Communication (ECOC)*, (2018).
2. J. . Cai, H. G. Batshon, M. V. Mazurczyk, O. V. Sinkin, D. Wang, M. Paskov, W. Patterson, C. R. Davidson, P. Corbett, G. Wolter, T. Hammon, M. Bolshtyansky, D. Foursa, and A. Pilipetskii, "70.4 Tb/s capacity over 7,600 km in C+L band using coded modulation with hybrid constellation shaping and nonlinearity compensation," in *Optical Fiber Communications Conference (OFC)*, (2017).
3. J. Cai, Y. Sun, H. Zhang, H. G. Batshon, M. V. Mazurczyk, O. V. Sinkin, D. G. Foursa, and A. Pilipetskii, "49.3 Tb/s transmission over 9100 km using C+L EDFA and 54 Tb/s transmission over 9150 km using hybrid-Raman EDFA," J. Light. Technol. **33**, 2724–2734 (2015).
4. J. Cai, H. G. Batshon, M. V. Mazurczyk, O. V. Sinkin, D. Wang, M. Paskov, C. R. Davidson, W. W. Patterson, A. Turukhin, M. A. Bolshtyansky, and D. G. Foursa, "51.5 Tb/s capacity over 17,107 km in C+L bandwidth using single-mode fibers and nonlinearity compensation," J. Light. Technol. **36**, 2135–2141 (2018).
5. A. Sano, T. Kobayashi, S. Yamanaka, A. Matsuura, H. Kawakami, Y. Miyamoto, K. Ishihara, and H. Masuda, "102.3-Tb/s (224 × 548-Gb/s) C- and extended L-band all-Raman transmission over 240 km using PDM-64QAM single carrier FDM with digital pilot tone," Natl. Fiber Opt. Eng. Conf. p. PDP5C.3 (2012).
6. L. Galdino, D. Semrau, M. Ionescu, A. Edwards, W. Pelouch, S. Desbruslais, J. James, E. Sillekens, D. Lavery, S. Barnes, R. I. Killey, and P. Bayvel, "Study on the impact of nonlinearity and noise on the performance of high-capacity broadband hybrid Raman-EDFA amplified system," J. Light. Technol. **37**, 5507–5515 (2019).
7. M. Ionescu, D. Lavery, A. Edwards, E. Sillekens, D. Semrau, L. Galdino, R. I. Killey, W. Pelouch, S. Barnes, and P. Bayvel, "74.38 Tb/s transmission over 6300 km single mode fibre enabled by C+L amplification and geometrically shaped PDM-64QAM," J. Light. Technol. **38**, 531–537 (2020).
8. J. Renaudier, A. Arnould, D. L. Gac, A. Ghazisaeidi, P. Brindel, M. Makhsiyan, A. Verdier, K. Mekhazni, F. Blache, H. Debregeas, A. Boutin, N. Fontaine, D. Neilson, R. Ryf, H. Chen, M. Achouche, and G. Charlet, "107 Tb/s transmission of 103-nm bandwidth over 3×100 km SSMF using ultra-wideband hybrid Raman/SOA repeaters," Opt. Fiber Commun. Conf. (OFC) p. Tu3F.2 (2019).
9. J. Renaudier, A. C. Meseguer, A. Ghazisaeidi, P. Tran, R. R. Muller, R. Brenot, A. Verdier, F. Blache, K. Mekhazni, B. Duval, H. Debregeas,

M. Achouche, A. Boutin, F. Morin, L. Letteron, N. Fontaine, Y. Frignac, and G. Charlet, "First 100-nm continuous-band WDM transmission system with 115Tb/s transport over 100km using novel ultra-wideband semiconductor optical amplifiers," in *European Conference on Optical Communication (ECOC),* (2017).
10. F. Hamaoka, M. Nakamura, S. Okamoto, K. Minoguchi, T. Sasai, A. Matsushita, E. Yamazaki, and Y. Kisaka, "Ultra-wideband WDM transmission in S-, C-, and L-bands using signal power optimization scheme," J. Light. Technol. **37**, 1764–1771 (2019).
11. L. Galdino, A. Edwards, W. Yi, E. Sillekens, Y. Wakayama, T. Gerard, W. S. Pelouch, S. Barnes, T. Tsuritani, R. I. Killey *et al.*, "Optical fibre capacity optimisation via continuous bandwidth amplification and geometric shaping," IEEE Photonics Technol. Lett. **32**, 1021–1024 (2020).
12. B. J. Puttnam, R. S. Luís, G. Rademacher, M. Mendez-Astudilio, Y. Awaji, and H. Furukawa, "S, C and extended L-band transmission with doped fiber and distributed Raman amplification," Opt. Fiber Commun. Conf. (OFC) p. Th4C.2 (2021).
13. I. Roberts, J. M. Kahn, J. Harley, and D. W. Boertjes, "Channel power optimization of WDM systems following Gaussian noise nonlinearity model in presence of stimulated Raman scattering," J. Light. Technol. **35**, 5237–5249 (2017).
14. J. Kani, K. Hattori, M. Jinno, T. Kanamori, and K. Oguchi, "Triple-wavelength-band WDM transmission over cascaded dispersion-shifted fibers," IEEE Photonics Technol. Lett. **11**, 1506–1508 (1999).
15. T. Hoshida, T. Terahara, J. Kumasako, and H. Onaka, "Optical SNR degradation due to stimulated Raman scattering in dual-band WDM transmission systems and its compensation by optical level management," Fifth Asia-Pacific. Fourth Optoelectronics Commun. Conf. on Commun. **1**, 342–345 (1999).
16. P. Krummrich, E. Gottwald, A. Mayer, C.-J. Weiske, and G. Fischer, "Influence of stimulated Raman scattering on the channel power balance in bidirectional WDM transmission," Opt. Fiber Commun. Conf. (OFC), Int. Conf. on Integr. Opt. Opt. Fiber Commun. (IOOC) **2**, 171–173 (1999).
17. S. Nallaperuma, N. A. Shevchenko, and S. J. Savory, "Parameter optimisation for ultra-wideband optical networks in the presence of stimulated Raman scattering effect," in *International Conference on Optical Network Design and Modeling (ONDM),* (2021).
18. B. Correia, R. Sadeghi, E. Virgillito, A. Napoli, N. Costa, J. Pedro, and V. Curri, "Optical power control strategies for optimized C+L+S-bands network performance," in *Optical Fiber Communications Conference,* (2021).
19. H. Buglia, E. Sillekens, A. Vasylchenkova, W. Yi, R. Killey, P. Bayvel, and L. Galdino, "Challenges in extending optical fibre transmission bandwidth beyond C+L band and how to get there," in *International Conference on Optical Network Design and Modeling (ONDM),* (2021).
20. A. M. R. Brusin, M. R. Zefreh, P. Poggiolini, S. Piciaccia, F. Forghieri, and A. Carena, "Machine learning for power profiles prediction in presence of inter-channel stimulated Raman scattering," in *European Conference on Optical Communication (ECOC),* (2021).
21. B. Correia, R. Sadeghi, E. Virgillito, A. Napoli, N. Costa, J. Pedro, and V. Curri, "Power control strategies and network performance assessment for C+L+S multiband optical transport," J. Opt. Commun. Netw. **13**, 147–157 (2021).
22. D. Semrau, R. I. Killey, and P. Bayvel, "A closed-form approximation of the Gaussian noise model in the presence of inter-channel stimulated Raman scattering," J. Light. Technol. **37**, 1924–1936 (2019).
23. P. Poggiolini, "A generalized GN-model closed-form formula." arXiv: 1810.06545 [eess.SP] (2018).
24. D. Semrau, R. I. Killey, and P. Bayvel, "The Gaussian noise model in the presence of inter-channel stimulated Raman scattering," J. Light. Technol. **36**, 3046–3055 (2018).
25. M. Cantono, D. Pilori, A. Ferrari, C. Catanese, J. Thouras, J.-L. Augé, and V. Curri, "On the interplay of nonlinear interference generation with stimulated Raman scattering for QoT estimation," J. Light. Technol. **36**, 3131–3141 (2018).
26. U. C. de Moura, F. D. Ros, A. M. R. Brusin, A. Carena, and D. Zibar, "Experimental characterization of Raman amplifier optimization through inverse system design," J. Light. Technol. **39**, 1162–1170 (2021).
27. M. Soltani, F. Da Ros, A. Carena, and D. Zibar, "Distance and spectral power profile shaping using machine learning enabled Raman amplifiers," in *IEEE Photonics Society Summer Topicals Meeting Series (SUM),* (2021).
28. D. Semrau, E. Sillekens, P. Bayvel, and R. I. Killey, "Modeling and mitigation of fiber nonlinearity in wideband optical signal transmission," J. Opt. Commun. Netw. **12**, C68–C76 (2020).
29. P. Poggiolini, "The GN model of non-linear propagation in uncompensated coherent optical systems," J. Light. Technol. **30**, 3857–3879 (2012).
30. D. Semrau, E. Sillekens, R. I. Killey, and P. Bayvel, "A modulation format correction formula for the Gaussian noise model in the presence of inter-channel stimulated Raman scattering," J. Light. Technol. **37**, 5122–5131 (2019).
31. M. Zirngibl, "Analytical model of Raman gain effects in massive wavelength division multiplexed transmission systems," Electron. Lett. **34**, 789–790 (1998).
32. J. Kennedy and R. Eberhart, "Particle swarm optimization," Proc. ICNN'95 - Int. Conf. on Neural Networks **4**, 1942–1948 (1995).
33. S. Boyd, S. P. Boyd, and L. Vandenberghe, *Convex optimization* (Cambridge university press, 2004).
34. M. Secondini, "Chapter 20 - information capacity of optical channels," in *Optical Fiber Telecommunications VII,* A. E. Willner, ed. (Academic Press, 2020).
35. A. Alvarado, T. Fehenberger, B. Chen, and F. M. Willems, "Achievable information rates for fiber optics: Applications and computations," J. Light. Technol. **36**, 424–439 (2018).